Solid State Communications 251 (2017) 98–103

Contents lists available at ScienceDirect

Solid State Communications

journal homepage: www.elsevier.com/locate/ssc

Communication

First-principles study of Al_2Sm intermetallic compound on structural, mechanical properties and electronic structure

Jingwu Lin[a,b], Lei Wang[a,b], Zhi Hu[a,b,*], Xiao Li[a,b], Hong Yan[a,b]

[a] Department of Materials Processing Engineering, School of Mechanical and Electrical Engineering, Nanchang University, Nanchang 330031, China
[b] Key Laboratory of Light Alloy Preparation & Processing in Nanchang City, Nanchang 330031, China

ARTICLE INFO

Keywords:
A. Intermetallic
B. Crystal structure
C. Mechanical properties
D. Electronic structure
E. First-principles

ABSTRACT

The structural, thermodynamic, mechanical and electronic properties of cubic Al_2Sm intermetallic compound are investigated by the first-principles method on the basis of density functional theory. In light of the strong on-site Coulomb repulsion between the highly localized 4f electrons of Sm atoms, the local spin density approximation approach paired with additional Hubbard terms is employed to achieve appropriate results. Moreover, to examine the reliability of this study, the experimental value of lattice parameter is procured from the analysis of the TEM image and diffraction pattern of Al_2Sm phase in the AZ31 alloy to verify the authenticity of the results originated from the computational method. The value of cohesive energy reveals Al_2Sm to be a stable in absolute zero Kelvin. According to the stability criteria, the subject of this work is mechanically stable. Afterward, elastic moduli are deduced by performing Voigt-Reuss-Hill approximation. Furthermore, elastic anisotropy and anisotropy of sound velocity are discussed. Finally, the calculation of electronic density of states is implemented to explore the underlying mechanism of structural stability.

1. Introduction

Rare earth elements, a type of important alloying elements, have been widely used in improving the high temperature mechanical properties and corrosion resistance of Mg-Al series magnesium alloys for developing high performance magnesium alloys, such as engine cradle alloy AE44 (Mg-4Al-4RE, wt%) [1,2]. In recent years, the advantageous microalloying effects of the Mg-Al series magnesium alloys with the addition of Sm have attracted many researchers [3–6]. Son et al. [7] found that Al-Sm-rich intermetallic compounds in Mg-Al-Ca alloys are markedly closer to the stoichiometric composition of Al_2Sm. The Al_2Sm phase could cause heterogeneous nucleation in the Mg-6Al-0.6Zn alloys based on orientation relationship [8]. Simultaneously, the mechanical properties of the Mg-Al alloys modified with Sm at 20–175 °C were dramatically improved, this is due to that the high thermal stable $Al_{11}Sm_3$ (orthorhombic structure) and Al_2Sm (face-centered cubic structure) precipitates could effectively prohibit dislocation movement and grain boundary sliding [9]. In addition, Hu et al. reported the corrosion potential of the Al_2Sm phase in the hot-extruded AZ61 magnesium alloys is likely to exist between the β-$Mg_{17}Al_{12}$ and α-Mg, so reducing the corrosion potential between the β-$Mg_{17}Al_{12}$ and α-Mg and would lead to the improvement in the corrosion resistance of the alloys [10].

Owing to the importance of Al_2Sm relative to Mg-Al series magnesium alloys, a thorough understanding of the physical properties of the Al_2Sm phase is necessary and crucial. The detailed structures of the petaloid Al_2Sm phase were thoroughly studied using TEM by Yang et al. [11]. They found that the Al_2Sm phase in the die-cast Mg-4Al-4Sm-0.3Mn alloy composed of multiple (111) twins with the (111) plane serving as the twinning plane. At the same time, the shear modulus of the Al_2Sm phase was used to analyze the fracture model of the Al_2Sm phase in the ultrasonic filed [12]. Nevertheless, the structural, mechanical properties and electronic structure of Al_2Sm has yet to draw enough attention and the amount of available information for this compound is short. Hence, this lack of information exhorts us to probe into such properties here.

The density functional theory based first-principles method, as the preference of many researchers, is complimented as a powerful tool to investigate physical and chemical properties of crystal materials with very limited error. In this paper, structural, mechanical, elastic anisotropic and electronic properties will be discussed by performing first-principles calculation.

2. Computational methodology

All data in this work came from first-principles calculation which

* Corresponding author at: Department of Materials Processing Engineering, School of Mechanical and Electrical Engineering, Nanchang University, Nanchang 330031, China.
E-mail address: huzhi215@163.com (Z. Hu).

http://dx.doi.org/10.1016/j.ssc.2016.12.018
Received 13 September 2016; Received in revised form 23 December 2016; Accepted 23 December 2016
Available online 24 December 2016
0038-1098/

adopt Cambridge serial total energy package (CASTEP) code [13] and which is performed by utilizing ultra-soft pseudopotential [14] on the basis of density functional theory (DFT) [15,16]. Valence electrons for distinct atoms of the studied system is Al 3s2 3p1 and Sm 4f6 5s2 5p6 6s2. In corresponding ground state, Sm donates 3 electrons to Al ions and therefore in trivalent (Sm^{3+}) configuration, the remaining 4f electrons are strongly localized. On account of the strong on-site Coulomb repulsion between highly localized 4f-electrons for Sm atoms, the conventional LDA or GGA method cannot describe the electronic localization effects or output reliable ground state properties. Therefore, the local spin density approximation (LSDA) approach paired with additional Hubbard terms (LSDA+U) was adopted to describe on-site electron-electron repulsion associated with the 4f narrow bands. In the present calculation, the value of cut-off energy for plane-wave was selected as 420.0 eV and the grid size applied to k-point sampling task in Brillouin zone (BZ) was selected as 5×5×5 by performing the Monkhorst-Pack scheme [17] which give good convergence. The evaluation of energy and stress was obtained by using the Pulay density mixing scheme [18]. The minimization scheme in geometry optimization is chosen as Broyden-Fletcher-Goldfarb-Shanno (BFGS) [19]. All atomic coordinates in the model are fully relaxed within the difference of total energy less than 5×10^{-6} eV the maximum stress less than 0.02 GPa. the maximum ionic Hellmann-Feynman force less than 0.01 eV/Å, and the maximum ionic displacement less than 5×10^{-4} Å. The calculation of total energy, elastic constants and electronic structure lie behind the work of geometry optimization with SCF tolerance of 5×10^{-7} eV. The elastic constants of Al_2Sm were determined by stress-strain method [20]. Furthermore, to examine the reliability of the methodology, an additional close related system (Al_2La) is investigated with the same methodology; hence it is viable to verify the authenticity of calculated results about Al_2Sm and bring about advantages in better illustrating features of properties of Al_2Sm.

3. Results and discussion

3.1. Crystal structure and lattice parameter

The Al_2Sm compound has the same crystal structure with Al_2La, which belongs to the cubic crystal system with space group F*d*-3*m* (No. 227), while the corresponding Wyckoff position of Al and Sm (La) atoms are 16d (5/8, 5/8, 5/8) and 8a (0, 0, 0). The model is shown in Fig. 1.

To dig into the ground state properties of the subject, the premier work is to evaluate the equilibrium lattice parameter. The value of this parameter was obtained after exercising the geometry optimization task. In the middle of this process, the total energy as a function of volume was calculated and fitted by the modified Birch-Murnaghan equation of state (EOS) [21–23]:

$$E(V) = a_1 + a_2 V^{-2/3} + a_3 V^{-4/3} + a_4 V^{-2}$$

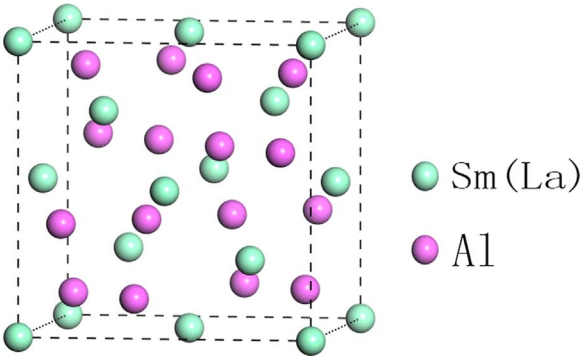

Fig. 1. Crystal structure of Al_2RE (RE=Sm or La) intermetallic compound.

Table 1
The calculated lattice constants a (Å), formation enthalpy ΔH (eV/atom) and cohesive energy E_{coh} (eV/atom) of Al_2Sm.

Species	Crystal system	Space group (#)	Pearson symbol	Lattice constants (a)	E_{coh}	ΔH
Al_2Sm	Cubic	FD–3M (227)	CF24	8.035	−9.490	−0.303
Al_2La				8.044	−5.055	−0.453

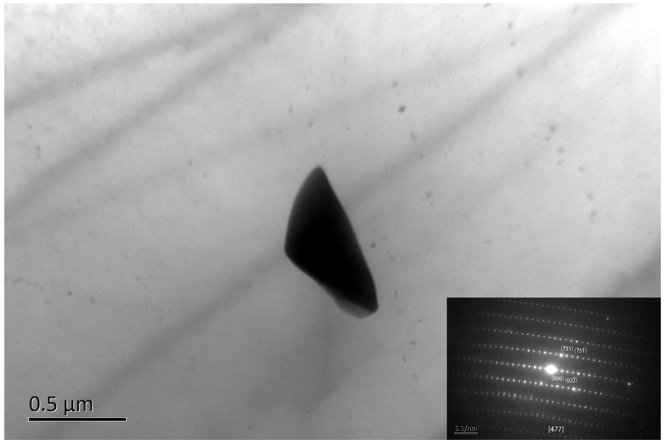

Fig. 2. The TEM image and diffraction pattern of Al_2Sm phase in the AZ31 alloy.

where a_i (i=1, 2, 3, 4) denote fitting parameters and the equilibrium lattice parameter (Table 1) at ground state.

Experimental value of lattice parameter of Al_2Sm is deduced from the analysis of the TEM image and diffraction pattern of Al_2Sm phase in the AZ31 alloy (Fig. 2). By comparing this with the experimental value of the lattice parameter of Al2Sm (7.940 Á) and Al_2La (8.148 Á [24]), it is discernible that the calculated value is consistent with the experimental one with the maximum deviation of less than approximately 1.3%, which confirm the reliability of the calculation and the methodology it embraces.

3.2. Structural stability and alloying ability

In order to study the structural stability and alloying ability of Al_2Sm, formation enthalpy and cohesive energy, as the respective measurement of the two properties, were calculated. Accordingly, the formation enthalpy (ΔH) and cohesive energy (E_{coh}) for Al_2Sm and Al_2La phase can be expressed as formula [25,26]:

$$\Delta H = \frac{1}{x+y}(E_{tot} - xE^{Al}_{solid} - yE^{RE}_{solid})$$

$$E_{coh} = \frac{1}{x+y}(E_{tot} - xE^{Al}_{atom} - yE^{RE}_{atom})$$

where E_{tot} symbolize total energy of unit cell, E^{Al}_{solid} and E^{RE}_{solid} stand for energy per atom of Al and RE (Sm or La) in solid states, E^{Al}_{atom} and E^{RE}_{atom} denote the energy of isolated Al atoms and RE atoms in free states and x (or y) refers to the number of Al (or RE) atoms. The calculated cohesive energy (Table 1) of both compounds is under −4 eV which express that both compounds are stable in ground state. Additionally, Al_2Sm has lower cohesive energy comparing with Al_2La; it reveals that Al_2Sm is more structurally stable than Al_2La. On the other side, Negative value of formation energy (Table 1) demonstrates an exothermic process and the energy stability. Concurrently, as the formation energy of Al_2Sm is higher than that of Al_2La, this indicates that Al_2Sm has a weaker alloying ability.

Table 2
The calculated f-state occupation n and spin magnetic moment m_{spin} (μ_B) of Al_2Sm for a series of U (eV) value.

U	3.0	4.0	5.0	6.0	7.0	8.0	9.0
n	5.94	5.95	5.96	5.99	6.00	6.00	6.00
m_{spin}	12.33	12.47	12.43	12.51	12.48	12.50	12.51

3.3. Mechanical properties

To examine the ideal U value, a series of U value are applied to obtain the respective f-state occupation numbers and spin magnetic moment as listed in the Table 2. It is noticeable that n and m_{spin} remain stable since U=6 eV. Thus, 6 eV is selected for U value.

Elastic constants indicate the resistance of materials to external force and are closely related to bonding characteristics, anisotropic and hardness. During the computing process, a series of small strain which meet the applicable condition of Hookie's law are imposed to the crystal structure to calculate the responding vacillation of stress and total energy. The total energy can be expressed with a Taylor series [27]:

$$E(v, \varepsilon) = E(V_0, 0) + V_0 \sum_{i=1}^{6} \sigma_i \varepsilon_i + \frac{V_0}{2} \sum_{i,j=1}^{6} C_{ij} e_i e_j + \ldots$$

where V_0 stands for volume of unstrained crystal and the respective energy of it is $E(V_0, 0)$. σ, C_{ij} and ε_i {e_i, e_j, ...} refers to stress tenor, single-crystal elastic constant and strain tenor. For cubic crystal system, only three (C_{11}, C_{12}, C_{44}, (C_{33}=C_{11}, C_{13}=C_{12}, C_{66}=C_{44})) independent elastic constants should be considered. The calculated results are displayed in Table 3 and could be used to measure the mechanical stability. For systems with cubic lattice symmetry, the elastic constants must fulfill the following criteria to be considered mechanically stable [28]:

$$C_{11} > 0,\ C_{44} > 0,\ C_{11} > |C_{12}|,\ (C_{11} + 2C_{12}) > 0$$

The structures of both precipitates are verified according to the criteria, and it so happens that both Al_2Sm and Al_2La are stable which is consistent with the analysis inferred from cohesive energy. Moreover, it is notable that the value of C_{11} is exceptionally high compared with others. This indicates that the structures are exceedingly incompressible under normal stress.

Compared with single-crystal elastic constants, the polycrystalline elastic properties such as shear modulus (G), bulk modulus (B), Young's modulus (E), and Poisson's ratio (v) are more widely used to characterize mechanical properties. According to the calculated elastic constants (C_{11}, C_{12} and C_{44}), the B and G are determined by the Voigt-Reuss-Hill (VRH) approach [29–31]:

$$G_H = (G_V + G_H)/2,\ B_H = (B_V + B_R)/2$$

where the subscripts V and R symbolize the Voigt and the Reuss approximations, respectively. Suitably, the Voigt and the Reuss approximations provide the upper and lower bound of bulk modulus plus shear modulus. The formula used to describe the various bounds with the class of crystal system. For cubic system, the Voigt bounds and the Reuss bounds of G and B (Table 3) are

Table 3
The calculated elastic constants (GPa), elastic moduli (GPa) and Poisson's ratios of Al_2Sm and Al_2La from first-principles calculation at 0 K.

Species	C_{11}	C_{12}	C_{44}	B_H	G_H	B_H/G_H	E	ν
Al_2Sm	100.84	22.31	38.23	48.49	38.64	1.26	91.59	0.185
Al_2La	150 61	35.45	43.44	73.83	48.63	1.52	119.64	0.230

$$G_V = (C_{11} - C_{12} + 3C_{44})/5,\ G_R = 5(C_{11} - C_{12})C_{44}/(4C_{44} + 3(C_{11} - C_{12})),$$
$$B_V = B_R = (C_{11} + 2C_{12})/3$$

Furthermore, Young's modulus (E) and Poisson ratio (ν) can be derived from Hill's bulk modulus (B_H) and shear modulus (G_H), for which the formula is

$$E = 9B_H G_H/(3B_H + G_H),\ \nu = (3B_H - 2G_H)/2(3B_H + G_H).$$

The calculated results are displayed in Table 3.

The calculated results are displayed in Table 3. It is discernable that all of the bulk modulus, shear modulus and Young's modulus of Al_2Sm are less than that of Al_2La; demonstrates that Al_2La has a better capacity to resist volume change and plastic deformation, and additionally a higher stiffness.

In addition, the ratio of bulk modulus to shear modulus (B_H/G_H) proposed by Pugh [32] is related with brittleness and ductility, and the criteria value of the ratio to separate them is 1.75 roughly [33]. A B/G ratio higher than the criteria indicates ductile material. Otherwise, the material tends to behave in a brittle manner. The B_H/G_H value are calculated and listed in Table 3. It comes about that the ratios of both compounds are less than 1.75; therefore categorizing both Al_2Sm and Al_2La as brittle materials.

Finally, the Poisson ratio ν is used to define the stability of the crystal against shear deformation. Usually the value of the index ranges from −1 to 0.5, a higher ν value denotes a higher plasticity and vice versa, this verifies that Al_2Sm has a junior plasticity than that of Al_2La. Simultaneously, the ν value for pure covalent, ionic and metallic materials are, in turn, 0.1, 0.25 and 0.33 [34], suggesting Al_2Sm and Al_2La to be ionic-covalent crystals.

3.4. Elastic anisotropy

Elastic anisotropy has extensive application in engineering science, for it is closely correlated with the possibility of inducing microcracks in materials [35]. The method used to measure the elastic anisotropy is the percentage of anisotropy in compression A_B and shear A_G, which is calculated by the following equations [36]:

$$A_B = (B_V - B_R)/(B_V + B_R),\ A_G = (G_V - G_R)/(G_V + G_R),$$

The value of anisotropy in compression and shear ranges from 0% to 100%. If A_B=A_G=0, it means the crystal is isotropy, while A_B=A_G=100% represents maximum elastic anisotropy [37]. The calculated results are listed in Table 4. This shows that Al_2Sm is isotropy in shear and compression, while Al_2Sm displays a small degree of anisotropy in shear but still isotropy in compression.

To illustrate the anisotropic characteristics of Al_2Sm and Al_2La more intuitively, a three-dimensional (3D) curved surface representation of the elastic anisotropy of both crystals were delineated. The 3D directional dependence of Young's modulus are derived from the relation [38]:

$$1/E = S_{11} - 2(S_{11} - S_{12} - S_{44}/2)(l_1^2 l_2^2 + l_2^2 l_3^2 + l_3^2 l_1^2)$$

where S_{ij} is elastic compliance constant (Table 4), and l_1, l_2 and l_3 are direction cosine in sphere coordination. The calculated results are displayed in Fig. 3. It shows that the 3D figure for Al_2Sm highly resembles a spherical shape. However, the profile for Al_2La phase

Table 4
The elastic compliance (1/GPa) and the percentage of anisotropy in the compression A_B (%) and shear A_G (%) of Al_2Sm and Al_2La.

Species	Elastic compliances (S_{ij})			A_B	A_G
	S_{11}	S_{12}	S_{44}		
Al_2Sm	0.010782	−0.001954	0.026157	0	0
Al_2La	0.007294	−0.001390	0.023020	0	0.950

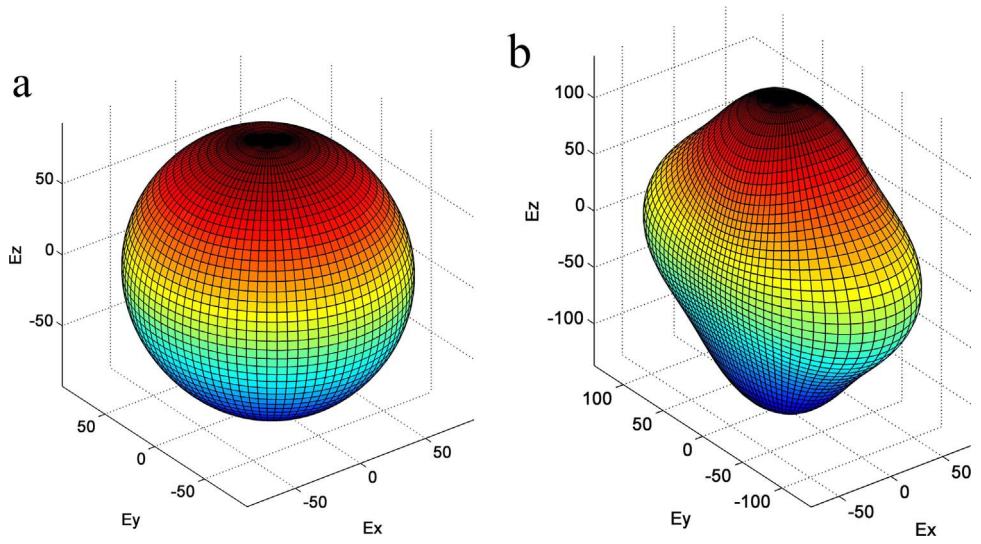

Fig. 3. Directional dependence of Young's modulus in Al_2Sm (a) and Al_2La (b), the units are in GPa.

exhibits a relatively obvious deviation from a spherical shape. Therefore, Al_2Sm shows perfect isotropy in Young's modulus, while Al_2La is obviously anisotropic.

3.5. Anisotropy of sound velocity and Debye temperature

By utilizing the calculated elastic constants, elastic wave velocities can be derived. The dependence of sound velocity on different directions of propagation are given by the equation [39]:

$$(\Lambda_{ij} - \rho V^2 \delta_{ij}) u_j = 0,\ \Lambda_{ij} = \sum_{k=1}^{3}\sum_{m=1}^{3} C_{ijkm} l_k l_m,$$

where the C_{ijkm} is the fourth rank tensor description of single crystal elastic constants, l_k and l_m symbolize directional cosines of propagation direction, u_j denotes polarization factor, ρprepresents mass density, and V is sound velocity. There are two types of solutions to this equation, namely a longitudinal wave (V_L) and two traverse waves (V_{T1}, V_{T2}) whose polarizations respectively run parallel and perpendicular to the direction of propagating. The factors that could influence the result of sound velocities are symmetry of crystal and direction of propagation. At the present work, only pure propagation modes ([1 0 0], [1 1 0], [1 1 1]) are investigated. For cubic system, sound velocity could be expressed by formula [40]:

$V_{T1}[1\,0\,0] = V_{T2}[1\,0\,0] = \sqrt{C44/\rho}$, $V_L[1\,0\,0] = \sqrt{C_{11}/\rho}$

$V_{T1}[1\,1\,0] = \sqrt{C_{44}/\rho}$, $V_{T2}[1\,1\,0] = \sqrt{(C_{11} - C_{12})/\rho}$,

$V_L[1\,1\,0] = \sqrt{(C_{11} + C_{12} + 2C_{44})/\rho}$,

$V_{T1}[1\,1\,1] = V_{T2}[1\,1\,1] = \sqrt{(C_{11} - C_{12} + C_{44})/3\rho}$,

$V_L[1\,1\,1] = \sqrt{(C_{11} + 2C_{12} + 4C_{44})/3\rho}$.

The calculated anisotropy sound velocities are tabulated in Table 5. Formulas above demonstrate that the precipitate with larger elastic constants and smaller density tend to exhibit larger sound velocity. In the meantime, it is easy to find that the longitudinal waves of both compounds are faster than its traverse wave. For both Al_2Sm and Al_2La, the fastest longitudinal wave is along [1 0 0] and the fastest traverse wave is along [1 1 0]. Moreover, as anisotropic sound velocities are associated with elastic anisotropy, prediction of it would be favorable to the further study of elastic anisotropy.

Table 5
The phonon velocities (m/s) of different directions, mass density $\rho(g/cm^3)$ and Debye temperature (K) of Al_2Sm and Al_2La.

Species	ρ	V_L^{100}	v_T^{100}	V_L^{110}	V_{T1}^{110}	V_{T2}^{110}	V_L^{111}	V_T^{111}	Θ_D
Al_2Sm	5.21053	4399	2709	4377	2709	3882	4369	2733	321
Al_2La	4.62426	5707	3065	5432	3065	4990	5338	3381	374

Debye temperature (Θ_D) is a fundamental parameter to describe the phenomena of solid-state physics. It defines a division line between classical and quantum-mechanical behavior of phonons. Additionally, it is widely accepted that quantum effect is obvious when temperature is below the threshold value of Θ_D, while it could be neglected when the temperature is above it [41]. The parameter is related to elastic constants, specific heat and melting temperature. Since the vibration excitations arise solely from acoustic vibrations at low temperature, Θ_D can be predicted from further analysis elastic constants, which is the same as when it is deducted from specific heat. The parameter is generally estimated, as one of standard method, by the formula [42]:

$$\Theta_D = \frac{h}{k_B}\left[\frac{3n}{4\pi}\left(\frac{N_A\rho}{M}\right)\right]^{1/3} V_m$$

where h, k_B, n, N_A, ρ and M represents Planck's constant, Boltzmann's constant, number of atoms per formula unit, Avogadro's number, mass density, molecular weight, respectively. V_m indicates the average sound velocity and it is defined as:

$$V_m = \left[\frac{1}{3}\left(\frac{2}{V_t^3} + \frac{1}{V_l^3}\right)\right]^{-1/3}$$

where V_l and V_t (Table 5) symbolize average longitudinal and traverse sound velocities, which are related with the elastic constants and the mass density as [43]:

$$V_l = \sqrt{[C_{11} + 2/5(2C_{44} + C_{12} - C_{11})]/\rho}$$
$$V_t = \sqrt{[C_{44} - 1/5(2C_{44} + C_{12} - C_{11})]/\rho},$$

According to empirical rule, a higher Debye temperature signifies a higher associated thermal conductivity plus a higher strength of chemical bonding. Comparing the Debye temperature of two compounds listed in Table 5, it is conspicuous that the Debye temperature of Al_2Sm is lower than that of Al_2La. Consequently, the conclusion that Al_2Sm has a relatively lower thermal conductivity and weaker chemical bonding than that of Al_2La can be obtained. To our knowledge, there is no existing information about the Debye temperature of Al_2Sm. Thus, our work can be valuable to other deeper studies.

3.6. Electronic structure

The density of states (DOS) is a quantity of illustrating the bonding

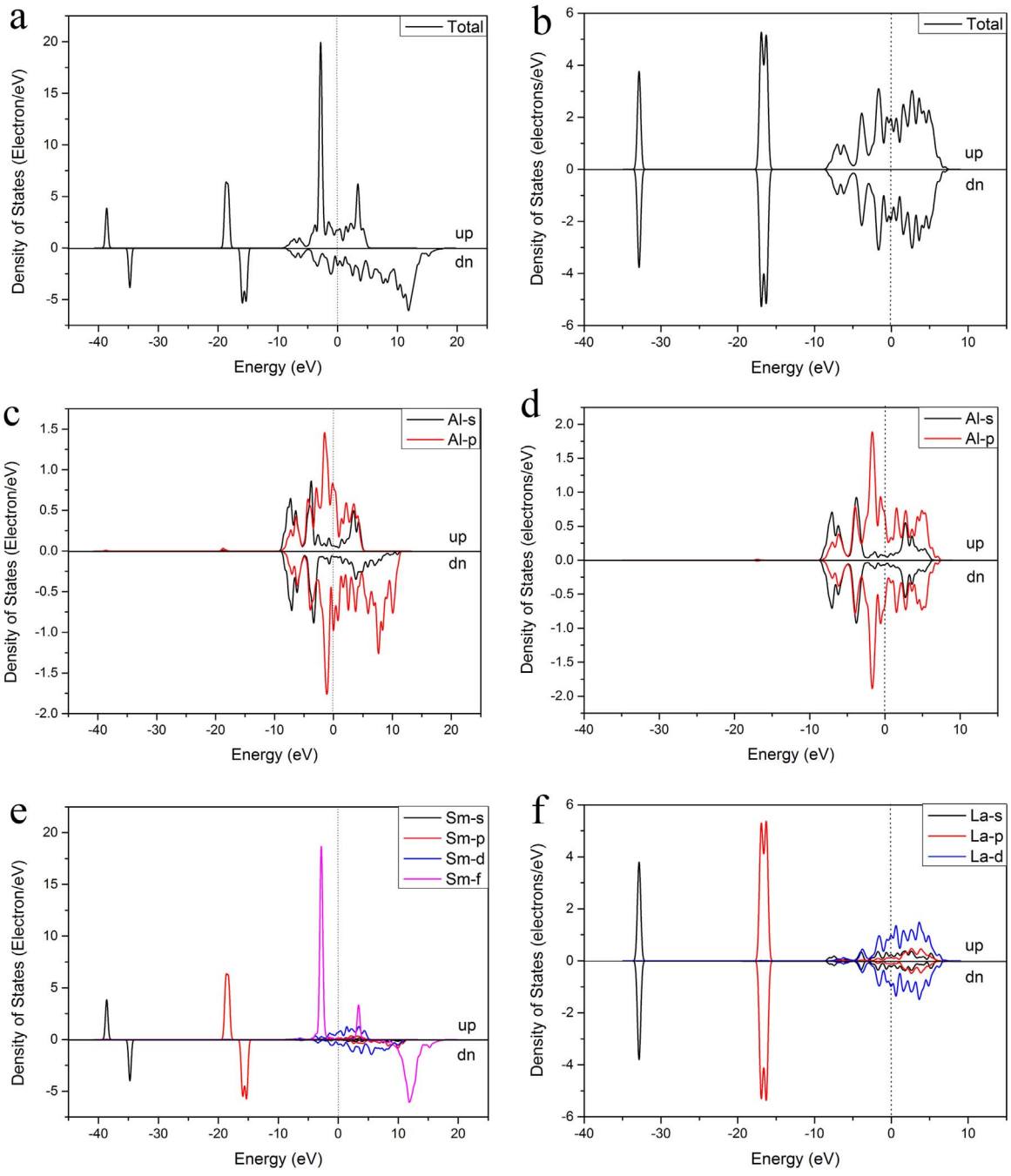

Fig. 4. Calculated total and partial density of states of Al_2Sm (a, c, e) and Al_2La (b, d, f), the vertical dotted line represents the Fermi energy level.

characteristics a compound holds. (TDOS) and partial density of states (PDOS) are calculated after geometry optimization process by the LSDA+U (U=6.0 eV) approach.

The results obtained are displayed in Fig. 4 where the vertical dotted line symbolizes Fermi energy. It is noticeable that the DOS for Al_2Sm shows four clear features. Firstly, the low-lying DOS (below −9 eV) mostly comes from the Sm-s and Sm-p states and hybridizes weakly with other orbits, which resemble that (La-s and La-p) of Al_2La; the difference is that spin-up and spin-down channels of Sm-s and Sm-p split strongly while that of La-s and La-p demonstrate nearly symmetrically. Secondly, the density of states at Fermi level contributes primarily from the hybridization of Sm-d and Al-p. Thirdly, TDOS of Al_2Sm shows a steep peak of f-electrons; on the contrary, there is no existence of f-electrons in that of Al_2La, for 4f orbit of La is totally unoccupied. In another work [44], the location of Sm-4f states is considerably deeper. This difference partly originates from the difference in the parameterization of exchange-correlation is different: we are using CA-PZ while [44] is using PBE. Another reason is that [44] uses FLAPW method. Since FLAPW is in principle more accurate than the pseudo-potential method, the position of Sm-4f states in our result might not be very accurate. However, the possible inaccuracy in the position of Sm-4f states does not change the conclusion of our study because they are located far below the Fermi level. Finally, the DOS structure show that there is no energy gap near Fermi level, it demonstrates that both Al_2Sm and Al_2La should exhibit a metallic character.

In addition, results from linear integral of DOS reveal that the number of bonding electron per atom of Al_2Sm at low energy level (−10–0 eV) is 4.66, which is higher than that (3.00) of Al_2La. Due to the charge interaction among bonding atoms largely has to do with

stability of the compound and the higher number of bonding electrons indicates higher stability [45], the Al_2Sm thus has a higher structural stability than Al_2La. This conclusion consists well with the prediction from the analysis of cohesive energy in the former section.

4. Conclusions

In summation, we have implemented extensive first-principles study on the structural, mechanical and electronic properties of cubic Al_2Sm along with Al_2La. It is notable that most results of physical properties of Al_2Sm are first-hand information. The calculated lattice parameters incorporate well within experimental value. Both Al_2Sm and Al_2La are mechanically stable according to the criteria of mechanical stability and Al_2Sm tends to be more stable than Al_2La. Elastic moduli are deduced and the ratio of bulk modulus to shear modulus (B_H/G_H) reveals that both compounds are brittle materials. Additionally, the mechanical anisotropy is estimated by calculating the percentage of anisotropy in compression and shear. The results show that the Al_2Sm phase has a higher degree of isotropy in shear. Furthermore, the Debye temperature of both compounds is predicted and we found that the value of it in Al_2Sm is lower than that of Al_2La, indicating that Al_2Sm has a more ordinary thermal conductivity than Al_2La. Finally, the electron structure is investigated to analyze the bonding characteristics.

Acknowledgment

The authors would like to acknowledge the financial support by the National Natural Science Foundation of China (51405216), the Natural Science Foundation of Jiangxi Province (20151BAB216018) and Training Program Foundation for Young Scientist of Jiangxi Province (20153BCB23023).

References

[1] M. Pekguleryuz, M. Celikin, Int. Mater. Rev. 55 (2010) 197–217.
[2] Q. Yang, X.J. Liu, F.Q. Bu, F.Z. Meng, T. Zheng, D.P. Zhang, J. Meng, Intermetallics 60 (2015) 92–97.
[3] C.L. Wang, J.C. Dai, W.C. Liu, L. Zhang, G.H. Wu, J. Alloy. Compd. 620 (2015) 172–179.
[4] D.G. Wu, S.H. Yan, Z.Q. Wang, Z.Q. Zhang, R.Y. Miao, X.W. Zhang, D.H. Chen, J. Rare Earths 32 (2014) 663–671.
[5] J. Zheng, Q.D. Wang, Z.L. Jin, T. Peng, Mater. Sci. Eng. A 527 (2010) 1677–1685.
[6] M. Sun, X.Y. Hu, L.M. Peng, P.H. Fu, Y.H. Peng, Mater. Sci. Eng. A 620 (2015) 89–96.
[7] H.T. Son, J.S. Lee, D.G. Kim, J. Alloy. Compd. 473 (2009) 446–452.
[8] K.J. Li, Q.A. Li, X.T. Jing, J. Chen, X.Y. Zhang, Q. Zhang, Scr. Mater. 60 (2009) 1101–1104.
[9] J.L. Wang, L.D. Wang, Y.M. Wu, L.M. Wang, Mater. Sci. Eng. A 528 (2011) 4115–4119.
[10] Z. Hu, X. Li, Q. Hua, H. Yan, H.X. Qiou, X.M. Ruan, Z.H. Li, J. Mater. Res 30 (2015) 3671–3681.
[11] Q. Yang, K. Guan, X. Qiu, D.P. Zhang, S.H. Lv, F.Q. Bu, Y.Q. Zhang, X.J. Liu, J. Meng, Mater. Sci. Eng. A 675 (2016) 396–402.
[12] Z. Hu, X. Li, H. Yan, X.Q. Wu, Q. Hua, J.W. Lin, J. Alloy. Compd. 685 (2016) 58–64.
[13] M.D. Segall, P.J.D. Lindan, M.J. Probert, C.J. Pickard, P.J. Hasnip, S.J. Clark, M.C. Payne, J. Phys.: Condens. Matter 14 (2002) 2717–2744.
[14] D. Vanderbilt, Phys. Rev. B 41 (1990) 7892–7895.
[15] P. Hohenberg, W. Kohn, Phys. Rev. B 136 (1964) 384.
[16] W. Kohn, L.J. Sham, Phys. Rev. A 140 (1965) 1133–1138.
[17] H.J. Monkhorst, J.D. Pack, Phys. Rev. B 13 (1976) 5188–5192.
[18] B. Hammer, L.B. Hansen, J.K. Nøskov, Phys. Rev. B 59 (1999) 7413–7421.
[19] B.G. Pfrommer, M. Côté, S.G. Louie, M.L. Cohen, J. Comput. Phys. 131 (1997) 233–240.
[20] J. Feng, B. Xiao, R. Zhou, W. Pan, D.R. Clarke, Acta Mater. 60 (2012) 3380–3392.
[21] H. Zhang, S.L. Shang, Y. Wang, A. Saengdeejing, L.Q. Chen, Z.K. Liu, Acta Mater. 58 (2010) 4012–4018.
[22] S. Shang, A. Bottger, Acta Mater. 53 (2005) 255–264.
[23] S.L. Shang, Y. Wang, D.E. Kim, Z.K. Liu, Comput Mater. Sci. 47 (2010) 1040–1048.
[24] A.B. Rao, P. Kistaiah, R.N. Rajasekhar, K. Satyanarayana, J. Mater. Sci. Lett. 1 (1982) 432–434.
[25] B.R. Sahu, Mater. Sci. Eng. B 49 (1997) 74–78.
[26] N.I. Medvedeva, Y.N. Gornostyrev, D.L. Novikov, O.N. Mryasov, A.J. Freeman, Acta Mater. 46 (1998) 3433–3442.
[27] J.F. Nye, Physical Properties of Crystals: Their Representation by Tensors and Matrices, Oxford University Press, Great Britain, 1957.
[28] B.G. Pfrommer, M. Côté, S.G. Louie, M.L. Cohen, J. Comput. Phys. 131 (1997) 233–240.
[29] A. Reuss, Z. Angew, Math. Mech. 9 (1929) 49–58.
[30] R. Hill, Proc. Phys. Soc. A65 (1952) 349–354.
[31] W. Voigt, Lehrburch der Kristallphysik, Teubner, Leipzig, 1928.
[32] S.F. Pugh, Philos Magn, Ser 7 (45) (1954) 823–843.
[33] W. Feng, S. Cui, H. Hu, P. Feng, Z. Zheng, Y. Guo, Z. Gong, Physica B 405 (2010) 4294–4298.
[34] J. Haines, J.M. Leger, G. Bocquillon, Annu. Rev. Mater. Res. 31 (2001) 1–23.
[35] V. Tvergaard, J.W. Hutchinson, J. Am. Ceram. Soc. 71 (1988) 157–166.
[36] Z.S. Nong, J.C. Zhu, X.W. Yang, Y. Chao, Z.H. Lai, Y. Liu, Physica B 407 (2012) 4706–4711.
[37] H.B. Ozisik, K. Colakoglu, E. Deligoz, Comput. Mater. Sci. 51 (2012) 83–90.
[38] P. Ravindran, P. Vajeeston, R. Vidya, A. Kjekshus, H. Fjellvåg, Phys. Rev. B 64 (2001) 224509.
[39] K. Lau, A.K. McCurdy, Phys. Rev. B 58 (1998) 8980–8984.
[40] J. Feng, B. Xiao, C.L. Wan, Z.X. Qu, Z.C. Huang, J.C. Chen, R. Zhou, W. Pan, Acta Mater. 59 (2011) 1742–1760.
[41] Z.L. Lv, Y. Chen, X.R. Chen, G.F. Ji, J. Alloy. Compd. 515 (2012) 44.
[42] O.L. Anderson, J. Phys. Chem. Solids 24 (1963) 909–917.
[43] Cz Jasiukiewicz, V. Karpus, Solid State Commun. 128 (2003) 167–169.
[44] H.J. Gotsis, I.I. Mazin, Phys. Rev. B 68 (2003) 224427.
[45] F. Nyléna, F.J. Garcia, B.D. Mosel, R. Pöttgen, U. Häussermann, Solid State Sci. 6 (2004) 147–155.